

Colossal Magnetodielectric Effect in $\text{SmFe}_3(\text{BO}_3)_4$ Multiferroic

A. A. Mukhin^a, G. P. Vorob'ev^b, V. Yu. Ivanov^a, A. M. Kadomtseva^b, A. S. Narizhnaya^b,
A. M. Kuz'menko^a, Yu. F. Popov^b, L. N. Bezmaternykh^c, and I. A. Gudim^c

^a Prokhorov General Physics Institute, Russian Academy of Sciences, Moscow, 119991 Russia

e-mail: mukhin@ran.gpi.ru

^b Moscow State University, Moscow, 119992 Russia

^c Kirensky Institute of Physics, Siberian Branch, Russian Academy of Sciences, Krasnoyarsk, 880036 Russia

Received December 31, 2010; in final form, February 1, 2011

The colossal (more than threefold) decrease in the dielectric constant ϵ in the easy-plane $\text{SmFe}_3(\text{BO}_3)_4$ ferroborate in a magnetic field of ~ 5 kOe applied in the basal ab plane of the crystal has been found. A close relation of this effect to anomalies in the field dependence of the electric polarization has been established. It has been shown that this magnetodielectric effect is due to the contribution to ϵ from the electric susceptibility, which is related to the rotation of spins in the ab plane, arises in the region of the antiferromagnetic ordering $T < T_N = 33$ K, and is suppressed by the magnetic field. A theoretical model describing the main features of the behavior of ϵ and electric polarization in the magnetic field has been proposed, taking into account the additional anisotropy in the basal plane induced by the magnetoelastic stresses.

DOI: 10.1134/S0021364011050079

1. INTRODUCTION

Magnetoelectric materials, in particular multiferroics, in which magnetic and ferroelectric (dielectric) properties are interrelated, have recently attracted a great deal of attention [1]. The recent discovery of new classes of multiferroics with a modulated spin structure in which the ferroelectric ordering is improper and arises upon the magnetic ordering produced a new upsurge of interest in these compounds [2–5], because the magnetoelectric coupling in them is much stronger than in other magnetoelectric materials. In particular, this is indicated by the discovery of the reorientation of the electric polarization in the magnetic field and dielectric anomalies during phase transitions in multiferroics of this type (TbMnO_3 , DyMnO_3 , etc.) [6, 7]. The presence of the spontaneous electric polarization related to the magnetic structure, which may deviate from the equilibrium state under the action of the electric field, should lead to an additional contribution to the dielectric properties. A considerable value of this contribution should be expected at the high spontaneous polarization and low magnetic anisotropy of the system.

Rare-earth ferroborates $\text{RFe}_3(\text{BO}_3)_4$ ($\text{R} = \text{Y}, \text{La-Lu}$) having the trigonal crystal structure (space group $R\bar{3}2$), in which the easy-plane antiferromagnetic structures are implemented, provide good possibilities for searching for and studying these effects. These magnets have recently attracted great attention due to the discovery of multiferroelectric properties and various phase transitions in them [8–13]. The antiferromagnetic ordering of the Fe^{3+} ions occurs there below

$T_N \sim 30\text{--}40$ K, when the iron spins are oriented either along the trigonal c axis (the easy-axis structure) or in the basal ab plane (the easy-plane structure). The magnetic ordering is also induced in the R subsystem due to the $\text{R}-\text{Fe}$ exchange, which plays an important role in the stabilization of any magnetic structure and the formation of the magnetic and magnetoelectric properties.

It was recently established [13] that $\text{SmFe}_3(\text{BO}_3)_4$ ferroborate has an easy-plane magnetic structure and shows the noticeable spontaneous electric polarization and relatively high electric polarization induced by the magnetic field and the increase in ϵ at low temperatures. This indicates a strong magnetoelectric coupling in this ferroborate and the possibility of the manifestation of noticeable magnetodielectric effects in the magnetic field in $\text{SmFe}_3(\text{BO}_3)_4$. These effects are studied in the present work.

2. EXPERIMENTAL METHODS

We grew $\text{SmFe}_3(\text{BO}_3)_4$ single crystals by crystallization from solutions of melts. The dielectric properties (capacity and conductivity) and the electric polarization were studied on a precision LCR-meter (QuadTech model 1920) at the frequencies of 10–200 kHz and an electrometer (B7-45), respectively, in the static magnetic fields of up to 15 kOe at the temperatures of 4–300 K. Electrodes made of conducting silver paste were deposited on definite faces of the studied sample perpendicularly to the direction of the measurements. The dielectric constant in the submillimeter wave range was measured on a quasioptical

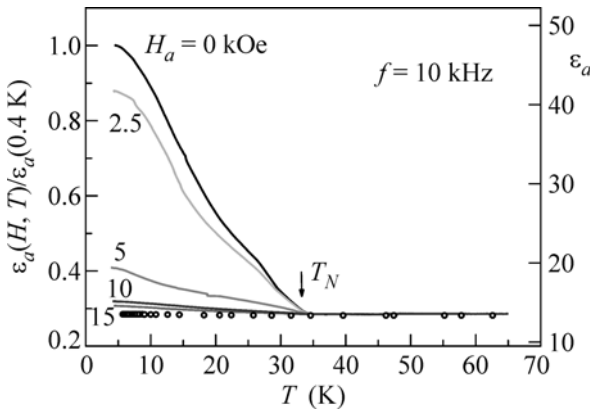


Fig. 1. Solid lines are temperature dependences of the real part of the dielectric constant ϵ_a along the a axis of the $\text{SmFe}_3(\text{BO}_3)_4$ crystal (at a frequency of 10 kHz) at different values of the magnetic field $H \parallel a$. Circles denote the submillimeter quasi-optical data at a frequency of 400 GHz at $H = 0$. The left-hand scale corresponds to the normalized radio-frequency permittivity and the right-hand scale gives the absolute values of the radio-frequency and submillimeter ϵ_a values.

spectrometer on the basis of the backward-wave tubes. Magnetic properties were studied in the static fields of up to 50 kOe on a SQUID magnetometer (MPMS-5, Quantum Design).

3. EXPERIMENTAL RESULTS

The temperature dependences of the real part of the dielectric constant ϵ_a along the a axis of the crystal at a frequency of 10 kHz are shown in Fig. 1. It is seen that the dielectric constant remains almost constant in the paramagnetic region, increases strongly with a decrease in the temperature below the Néel point, and at low temperatures is three times higher than its high-temperature value. The application of a rather low magnetic field in the basal ab plane leads to the strong decrease in ϵ_a as indicated by the relevant $\epsilon_a(T)$ dependences at different values of the magnetic field (Fig. 1). At the field ~ 15 kOe, the increase in $\epsilon_a(T)$ is almost completely suppressed. The frequency dependence of the dielectric constant is almost absent up to 200 kHz. However, according to the submillimeter studies, ϵ_a at high frequencies (200–400 GHz) has no anomalies below the Néel point and is close to the relevant value for 10–200 kHz in the paramagnetic region (Fig. 1). This allows one to localize the range of the frequency dispersion of ϵ in order to search for the resonance excitations determining the contribution to ϵ . This will be the subject of a separate study.

To study the effect of the magnetic field on the dielectric constant in more detail, the field dependences of $\epsilon_a(H_a)$ and $\epsilon_a(H_b)$ were measured (Fig. 2). Their common feature is a strong decrease in ϵ_a in a

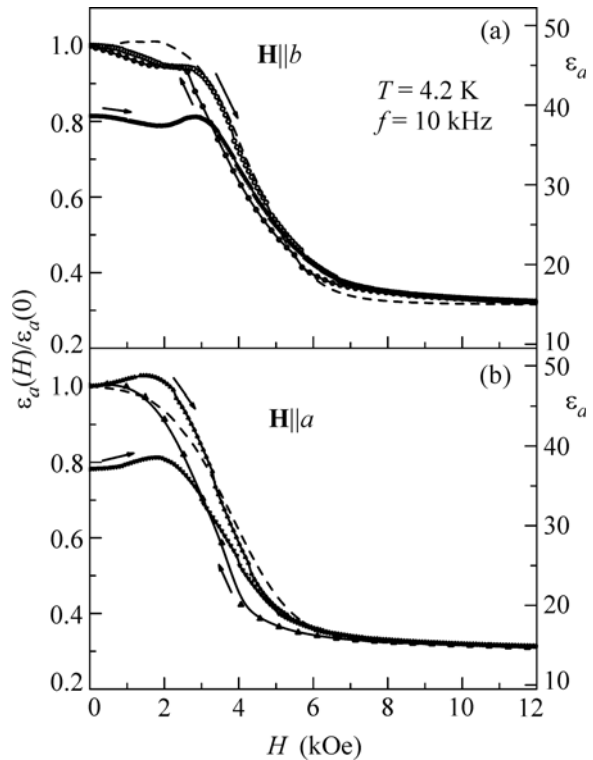


Fig. 2. Real part of the dielectric constant ϵ_a along the a axis of the $\text{SmFe}_3(\text{BO}_3)_4$ crystal (at a frequency of 10 kHz) versus the magnetic field intensity for the cases (a) $H \parallel b$ and (b) $H \parallel a$. The points and solid lines are the experimental data, whereas the dashed lines are the theoretical curves. The low-lying curve in each panel is obtained after the primary cooling of the sample in zero magnetic field.

field of ~ 4 – 5 kOe and its further smooth decrease to its high-temperature value. A noticeable hysteresis (~ 1 kOe) of the field dependences of ϵ is observed. Another feature of the behavior of ϵ is its dependence on the prehistory: upon the primary cooling of the sample from the paramagnetic state in the zero magnetic field, the ϵ_a value is about 20% lower than its value at $H = 0$ after the sample magnetization cycle (Fig. 2).

The comparison of the dielectric constant at different directions of the magnetic field shows that the characteristic threshold fields at which ϵ_a changes sharply are ~ 0.5 – 1 kOe less at $H \parallel a$ than at $H \parallel b$. In addition, the forms of the corresponding $\epsilon_a(H_a)$ and $\epsilon_a(H_b)$ curves differ. In some cases, they demonstrate the nonmonotonic behavior accompanied by the appearance of ϵ_a maxima. All these facts indicate the presence of the anisotropy in the basal plane and the strong relation of the dielectric constant to the magnetic structure, in particular the orientation of spins in the crystal ab plane.

To clarify these aspects in more detail, the electric polarization and magnetization (magnetic susceptibil-

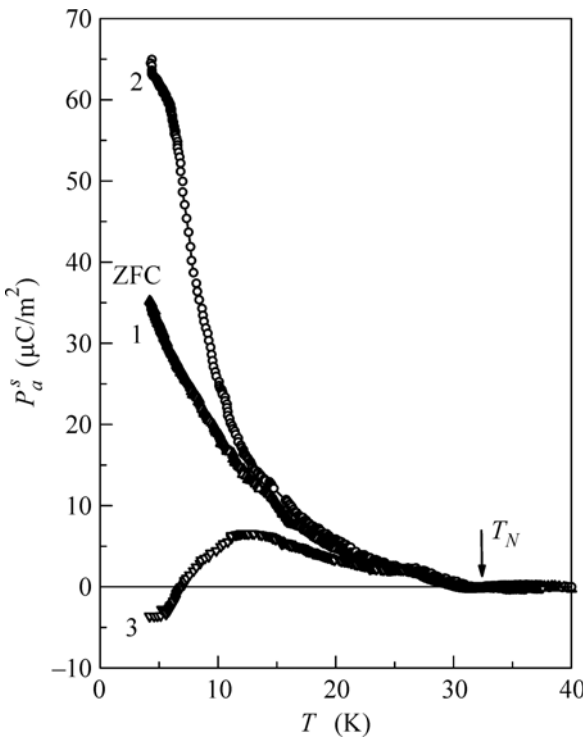


Fig. 3. Temperature dependences of the spontaneous electric polarization along the a axis of the $\text{SmFe}_3(\text{BO}_3)_4$ crystal at $H=0$ obtained under different conditions: line 1 corresponds to cooling in zero magnetic field, whereas lines 2 and 3 were obtained after preliminary application of a magnetic field of 13 kOe along the a and b axes, respectively.

ity) of $\text{SmFe}_3(\text{BO}_3)_4$ were studied. The behaviors of the spontaneous $P_a^s(T)$ and magnetic-field-induced $P_a(H_{a,b})$ electric polarizations are shown in Figs. 3 and 4, respectively. It is seen that cooling in the zero magnetic field below T_N is accompanied by the appearance of the electric polarization P_a^s , increasing with a decrease in the temperature (curve 1 in Fig. 3). The measurement of $P_a(H_a)$ in the state at $T=4.2$ K indicates a rather sharp increase in the polarization in the fields of 2–5 kOe and a gradual approach to the saturation in high fields (Fig. 4). When the field decreases, the hysteresis arises and the polarization at $H=0$ becomes larger than the initial value. Its temperature dependence follows line 2 in Fig. 3. The $P_a(H_b)$ dependence measured with the sample cooled again in the zero magnetic field from a temperature above T_N is similar to the $P_a(H_a)$ dependence but with the opposite sign. This corresponds to the phenomenological theory [8, 9], according to which $P_a \equiv P_x \sim (L_x^2 - L_y^2)$ and the P_a signs in two states $\mathbf{L} \perp \mathbf{a}$ and $\mathbf{L} \perp \mathbf{b}$ induced by the H_a and H_b fields, respectively, are opposite, where \mathbf{L} is the antiferromagnetic moment of the Fe^{3+} ions

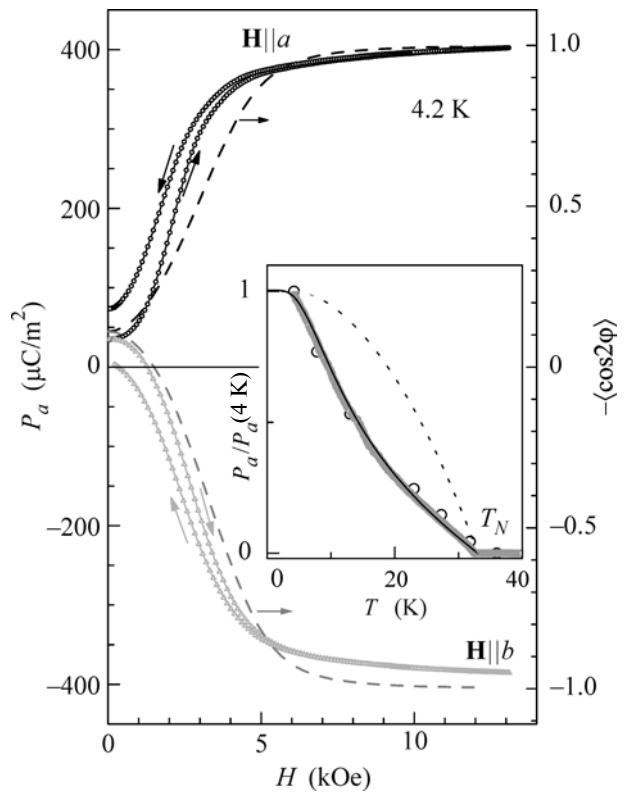


Fig. 4. Spontaneous electric polarization along the a axis of the $\text{SmFe}_3(\text{BO}_3)_4$ crystal versus the magnetic field intensity for the cases $\mathbf{H} \parallel a$ and $\mathbf{H} \parallel b$. The points are the experimental data (left scale) and the dashed line is the theoretical curve (right scale). The inset shows the temperature dependence of the polarization in the saturated state: the points are the experimental data (field of 7 and 10 kOe), whereas the solid and dashed lines are the theoretical curves including the rare-earth contribution and contribution of only the Fe subsystem, respectively.

and the x , y , and z axes coincide with a , b , and c axes, respectively. Since the spontaneous polarization is almost an order of magnitude lower than the field-induced polarization, the directions of spins (\mathbf{L}) are distributed rather homogeneously in the basal plane. The fact that the polarization change in the H_b field is larger than that in the H_a field indicates that the spins are on average closer to the b axis; i.e., $\langle L_y^2 \rangle > \langle L_x^2 \rangle$. However, this state can change depending on the pre-history. In particular, the spontaneous polarization differs from the initial value after the field is displaced from the induced $H \parallel b$ state and becomes close to zero or even negative (Fig. 4). This indicates the change in the spin distribution where $\langle L_y^2 \rangle < \langle L_x^2 \rangle$ already. Then, when the temperature increases, the spontaneous polarization in this state changes in another manner and follows line 3 in Fig. 3 that at $T \geq 15$ K approaches the initial curve marked by 1. This indicates that the magnetic state induced by $H \parallel b$ at low

temperatures is metastable and transforms at $T \geq 15$ K to a more stable state with $\langle L_y^2 \rangle > \langle L_x^2 \rangle$.

Note that the effect of the prehistory was also manifested in the temperature dependences of the magnetic susceptibility and magnetization curves in the basal plane. The magnetization changing the spin distribution or the ratio of the antiferromagnetic domains in the basal plane leads to the noticeable change in the values of the spontaneous polarization and magnetic susceptibility; this fact indicates that the appearance of the magnetization is determined by some factors lowering the crystal symmetry. The uniaxial anisotropy induced by the mechanical stresses due to the magnetoelastic interaction can be one of such factors [12, 13].

4. THEORY AND DISCUSSION OF THE RESULTS

To describe the observed dielectric and magnetoelectric properties of the system, let us consider its thermodynamic potential,

$$\Phi(\mathbf{I}, \mathbf{P}, \mathbf{H}, \mathbf{E}) = \Phi_m(\mathbf{I}, \mathbf{H}) + \Phi_{me}(\mathbf{I}, \mathbf{P}) + \Phi_e(\mathbf{P}, \mathbf{E}), \quad (1)$$

including the magnetic, $\Phi_m(\mathbf{I}, \mathbf{H})$, magnetoelectric, $\Phi_{me}(\mathbf{I}, \mathbf{P})$, and electric, $\Phi_e(\mathbf{P}, \mathbf{E})$, parts. The magnetic part is given by the expression

$$\begin{aligned} \Phi_m(\mathbf{I}, \mathbf{H}) = & -\frac{1}{2}\chi_\perp[\mathbf{H}^2 - (\mathbf{H}\mathbf{I})^2] + \frac{1}{2}K_{\text{eff}}l_z^2 \\ & + \frac{1}{12}K_6[(l_x + il_y)^6 + (l_x - il_y)^6] - \frac{1}{2}K_{1u}(l_x^2 - l_y^2) - K_{2u}l_xl_y, \end{aligned} \quad (2)$$

where the first term determines the energy of the antiferromagnet canting in the magnetic field, the second term is the energy of the uniaxial anisotropy stabilizing the easy *ab* plane ($K_{\text{eff}} > 0$), and the third and fourth terms are the energies of the crystallographic hexagonal anisotropy and magnetoelastic anisotropy $K_{1u} \sim \sigma_{xx} - \sigma_{yy}$, $K_{2u} \sim \sigma_{xy}$, respectively, which are induced by the internal stress of compression/elongation $\sigma_{xx} - \sigma_{yy}$ and shift σ_{xy} in the crystal *ab* plane. The part of the magnetoelectric interaction energy relevant to the present analysis related to the orientation of spins in the basal plane is [8, 9]

$$\Phi_{me}(\mathbf{I}, \mathbf{P}) = -c_2P_x(l_x^2 - l_y^2) + 2c_2P_yl_xl_y + \dots \quad (3)$$

The electric part of the thermodynamic potential is given by the expression

$$\Phi_e(\mathbf{P}, \mathbf{E}) = (P_x^2 + P_y^2)/2\chi_e^\perp + P_x^2/2\chi_e^\parallel - \mathbf{PE}, \quad (4)$$

where χ_e^\perp and χ_e^\parallel are the lattice components of the (di)electric susceptibility. For simplicity, the contribution of the Sm subsystem is not explicitly taken into account and it is assumed that the corresponding

parameters in Eqs. (1)–(3) (K_{eff} , K_u , c_2 , ...) are renormalized due to the Sm–Fe interaction.

Let us characterize the easy-plane antiferromagnetic structure of interest by the angle φ : $l_x = \cos\varphi$, $l_y = \sin\varphi$. By minimizing the thermodynamic potential Φ in Eq. (1) in \mathbf{P} and substituting the found expressions $P_x = P_\perp^0 \cos 2\varphi + \chi_e^\perp E_x$, $P_y = -P_\perp^0 \sin 2\varphi + \chi_e^\perp E_y$, where $P_\perp^0 = c_2\chi_e^\perp$ into it, we obtained the electric susceptibility (permittivity) χ_e^x along the *a* axis in the form

$$\begin{aligned} \chi_e^x & \equiv dP_x/dE_x = -\Phi_{E_x E_x} + (\Phi_{E_x \varphi})^2/\Phi_{\varphi \varphi} \\ & = \chi_e^\perp + (2P_\perp^0 \sin 2\varphi_0)^2/\Phi_{\varphi \varphi}, \end{aligned} \quad (5)$$

where $\Phi_{E_x E_x} = \partial^2 \Phi / \partial E_x^2$, $\Phi_{E_x \varphi_x} = \partial^2 \Phi / \partial E_x \partial \varphi$, $\Phi_{\varphi \varphi} = \partial^2 \Phi / \partial \varphi^2$, and the equilibrium value of the angle $\varphi = \varphi_0$ is determined by the equation $\partial \Phi / \partial \varphi = 0$. It is seen from Eq. (5) that an additional contribution to the electric susceptibility arises in the system, which is determined by the electric polarization P_\perp^0 in the basal plane and the rigidity $\Phi_{\varphi \varphi}^0$ with respect to the rotation of spins in this plane. This contribution is similar to the well-known magnetic susceptibility of rotation in ferromagnets or weak ferromagnets and, therefore, can analogously be called *electric susceptibility of rotation*. The rigidity (stability) of the equilibrium spin configuration is determined by the quantity $\Phi_{\varphi \varphi}^0 = 6K_6 \cos 6\varphi_0 + K_u \cos 2(\varphi_0 - \varphi_u) - \chi_\perp H^2 \cos 2(\varphi_0 - \varphi_H)$, which in the stable state should be positive, where $K_u^2 = K_{1u}^2 + K_{2u}^2$ and $\tan 2\varphi_u = K_{2u}/K_{1u}$.

First, the behavior of the electric susceptibility in the magnetic field is analyzed for the ideal crystal characterized only by the hexagonal crystallographic anisotropy in the *ab* plane. Let $K_6 > 0$ for definiteness. Then, at $H = 0$ there are three types of the equilibrium states (domains) $\varphi_1 = 0$ and $\varphi_{2,3} = \pm\pi/3$. Let $H \parallel a$ ($\varphi_H = 0$). Then, the state $\varphi_1 = 0$ remains the same until H_x reaches the value of the spin-flop transition, $H_0 = \sqrt{6K_6/\chi_\perp}$ when the antiferromagnetic moment \mathbf{L} rotates by 90° perpendicular to H and the angles in two other states $\sin 2\varphi_{2,3} = \pm\sqrt{1 - H_x^2/H_0^2}$ smoothly approach the directions orthogonal to the field at $H_x \rightarrow H_0$. The first state does not contribute to the dielectric constant and the contribution of the two other states in the angular phase ($H_x < H_0$) is $\Delta\epsilon_x(H_x) = \Delta\epsilon_x^0/\sqrt{1 + 3H_x^2/H_0^2}$ and $\Delta\epsilon_x(H_x) = 0$ at $H_x > H_0$, where $\Delta\epsilon_x^0 = 4\pi(2P_\perp^0)^2/8K_6$. The dependence $\Delta\epsilon_x(H_x)$ is shown in Fig. 5a, where the dotted line corresponds to the initial state with the equiprobable distribution over three domains $\varphi_{1,2,3}$ and the solid line corresponds to

more stable states $\varphi_{2,3}$ to which the system transforms at the magnetization cycle above H_0 .

At the other field direction, $H \parallel b$ ($\varphi_H = \pi/2$), the state $\varphi_1 = 0$ remains the same and in two other states $\cos 2\varphi_{2,3} = \frac{1}{2}\sqrt{1 - 3H_y^2/H_0^2}$ and the angles gradually

approach the value $\pm\pi/4$ at $H_y \rightarrow H_0/\sqrt{3}$, where the stability of the metastable $\varphi_{2,3}$ states is lost and the transition to the stable state $\varphi_1 = 0$ occurs where the system remains. The rotation dielectric contribution

$\Delta\epsilon_x(H_e) = \Delta\epsilon_x^0 / \sqrt{1 - 3H_y^2/H_0^2}$ differs from zero only for the metastable $\varphi_{2,3}$ states, diverges at $H_y \rightarrow H_0/\sqrt{3}$

upon the transition from the metastable angular phase to the state orthogonal to the field where it becomes zero (Fig. 5b). The magnetodielectric effect in this case is manifested only in the primary magnetization cycle when the corresponding metastable $\varphi_{2,3}$ states exist and it disappears at the transition of \mathbf{L} to the state orthogonal to the field.

Thus, the results obtained for purely hexagonal anisotropy demonstrate the presence of the magnetodielectric effect which, however, qualitatively differs at the magnetization along the crystal a and b axes. This is inconsistent with the experimental data demonstrating, on the contrary, a similar behavior of the dielectric constant in the field along both axes. To clarify the situation, the effect of the magnetoelastic energy of the anisotropy, $-K_u \cos 2(\varphi - \varphi_u)$, induced by the internal stress in the real crystal is considered. Locally, i.e., in the definite crystal region, this anisotropy is uniaxial with an easy axis in the basal plane determined by the angle φ_u . However, taking into account the random character of the distribution of the internal stresses, one should expect the corresponding distribution of both the directions of the easy axes φ_u and the anisotropy value K_u . Therefore, to find the magnetodielectric contribution to permittivity in this case, it is necessary to determine the local orientation \mathbf{l} , i.e., the angle φ and then to average the corresponding electric susceptibility given by Eq. (5) for the definite distribution of φ_u , K_u or K_{1u} , K_{2u} . Since the problem in the general case with both hexagonal and induced anisotropies is very intricate, only the induced magnetoelastic anisotropy is taken into account at this stage.

By minimizing the thermodynamic potential Eq. (2) in the angle φ at $H \parallel a$, the local equilibrium value $\tan 2\varphi = K_{2u}/(K_{1u} - \chi_\perp H_x^2)$ is found. When it is substituted into Eq. (5), the local magnetodielectric contribution

$$\Delta\epsilon_x(H_x) = \Delta\epsilon_x^0 \frac{\sin^2 2\varphi_u}{[1 - 2h_x^2 \cos 2\varphi_u + h_x^4]^{3/2}}, \quad (6)$$

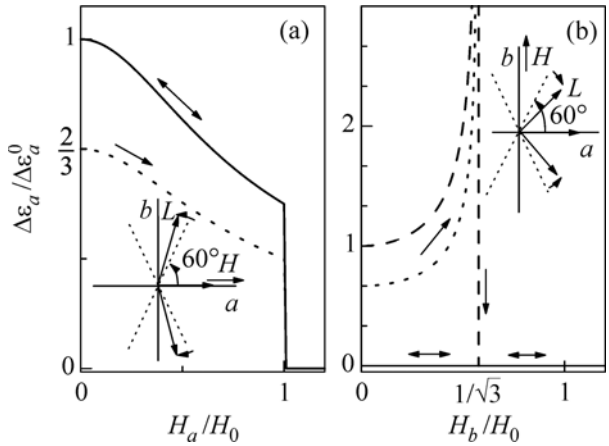


Fig. 5. Theoretical magnetic-field dependences of the rotational dielectric constant (electric susceptibility) in the case of the hexagonal crystallographic anisotropy in the ab plane at $\mathbf{H} \parallel a$ and $\mathbf{H} \parallel b$. The arrows in the insets show the deviation of \mathbf{L} in the field from the easy axes (dotted line) in different domains.

is obtained, where $\Delta\epsilon_x^0 = 4\pi(2P_\perp^0)^2/K_u$, $h_x^2 = \chi_\perp H_x^2/K_u$. Depending on the direction of the easy axis φ_u , $\Delta\epsilon_x(H_x)$ can either have a maximum ($\varphi_u < \pi/4$) or decrease monotonically ($\varphi_u > \pi/4$), and at high fields it decreases as $1/H_x^6$.

Let us assume that the K_{1u} and K_{2u} parameters of the induced anisotropy have the two-dimensional Gauss distribution and are characterized by the same variance ΔK_u^2 , mean values \bar{K}_{1u} and \bar{K}_{2u} , and the absence of correlation between K_{1u} and K_{2u} . The results of the numerical calculations and the simulation of the $\Delta\epsilon_x(H_x)$ and $\Delta\epsilon_x(H_y)$ dependences are given in Fig. 2 by dashed lines. It is seen that the observed field dependences are described on the whole within the present model. The distribution parameters found from the comparison with the experiment are $\Delta K_u = 5.5 \times 10^3$ erg/cm³, $\bar{K}_{1u} = -1.2 \times 10^3$ erg/cm³, and $\bar{K}_{2u} = 0$, where the \bar{K}_{1u} value is negative, because the easy axis of the induced anisotropy energy lies on the average along the b axis. This circumstance determines the threshold field value along the b axis as being somewhat larger than that along the a axis. Using the expression for the average magnetodielectric contribution $\Delta\epsilon_x^0 \approx 4\pi(2P_\perp^0)^2 \sqrt{\pi/2} / 2\Delta K_u \approx 32.5$ at $H = 0$ ($\Delta K_{1u} \gg |\bar{K}_{1u}|$, $|\bar{K}_{2u}|$), the polarization $P_\perp^0 = \chi_e^\perp c_2$ in the state $\mathbf{l} \perp \mathbf{H}$ was estimated as ≈ 255 $\mu\text{K/m}^2$, which has the same order as its direct measurement ~ 400 $\mu\text{K/m}^2$ (Fig. 4). The behavior of the electric polarization $P_x(H_{x,y}) = P_\perp^0 \langle \cos 2\varphi \rangle$ within the considered approach also agrees with the experiment (see the

dashed lines in Fig. 4). Thus, the proposed model taking into account the distributed character of the induced magnetoelastic anisotropy in the basal plane generally gives a consistent description of the field dependences of both the dielectric constant and polarization.

The temperature dependences are now discussed in short. The temperature dependence of the polarization in the saturated ($\mathbf{l} \perp \mathbf{H}$) state $P_{\perp}^0(T)$ is shown in the inset in Fig. 4. It is seen that the behavior of $P_{\perp}^0(T)$ definitely does not correspond to the contribution of only the Fe subsystem proportional to the square of the average value of its antiferromagnetism vector $L_0^2(T)$ (see the dashed line in the inset in Fig. 4, molecular field approximation). This indicates the prevailing contribution of the R subsystem to the polarization. The phenomenological analysis of the magnetoelectric interactions in ferroborates taking into account the contribution of the R subsystem is given in [9]. However, it includes a large number of constants, not all of which are relevant for the definite system. In this work, the rare-earth contribution was analyzed on the basis of the approach taking into account the features of the ground state of the R ion in a crystal (Kramers doublet) and the corresponding Hamiltonian of the magnetoelectric interaction for the R ion in analogy with the approach in [14–16] for the description of the magnetoelastic interactions in rare-earth magnets. As a result, the relevant contribution to the magnetoelectric interaction determined by the low-lying Kramers doublet of the R ion is

$$\begin{aligned}\Phi_{me}^R = & -P_x \{ c_{2R} [l_x(\sigma_x^+ - \sigma_x^-) - l_y(\sigma_y^+ - \sigma_y^-)] \\ & + c'_{2R} [H_x(\sigma_x^+ + \sigma_x^-) - H_y(\sigma_y^+ + \sigma_y^-)] \} \\ & - P_y \{ -c_{2R} [l_x(\sigma_y^+ - \sigma_y^-) + l_y(\sigma_x^+ - \sigma_x^-)] \\ & - c'_{2R} [H_x(\sigma_y^+ + \sigma_y^-) + H_y(\sigma_x^+ + \sigma_x^-)] \},\end{aligned}\quad (7)$$

where $\sigma_{x,y}^{\pm} = [(\mu_{\perp} H_{x,y} \pm \Delta_{\perp} l_{x,y})/\Delta^{\pm}] \tanh(\Delta^{\pm}/T)$ are the average values of the x and y components of the Pauli matrices of the ground doublet of the R ions in the sublattices \pm , respectively; $2\Delta^{\pm} = 2[(\mu_{\perp} H_x \pm \Delta_{\perp} l_x)^2 + (\mu_{\perp} H_y \pm \Delta_{\perp} l_y)^2]^{1/2}$ is the splitting of the doublet in the R–Fe exchange and external fields; μ_{\perp} is the magnetic moment (g factor) of the doublet in the basal plane; and c_{2R} and c'_{2R} are constants. Taking into account the specificity of the Kramers Sm^{3+} ion due to the weak interaction with the external field because of the low value of the Lande factor ($|\sigma_{x,y}^+ + \sigma_{x,y}^-| \ll |\sigma_{x,y}^+ - \sigma_{x,y}^-|$), it is possible to present Φ_{me}^R at $H_{x,y} \ll \Delta_{\perp}/\mu_{\perp}$ as Eq. (3), where the magnetoelectric constant depends on T as $c_{2R} L_0 \tanh[\Delta_{\perp} L_0/T]$. The solid line in the inset in Fig. 4

shows the calculated dependence $P_{\perp}^0(T)$, which describes the experiment well. The splitting value $2\Delta_{\perp} = 13 \text{ cm}^{-1}$ is taken from the optical data [17].

The observed temperature dependence $\varepsilon_a(T)$ is similar to the dependence $P_{\perp}^0(T)$ (Fig. 1) in spite of the fact that $\varepsilon_a(T)$ is proportional to the square of $P_{\perp}^0(T)$ (see Eqs. (5) and (6)). This indicates that the anisotropy energy in the ab plane also increases with the decrease in T according to the law similar to $P_{\perp}^0(T)$, apparently due to the rare-earth contribution, thus determining a smoother increase in $\varepsilon_a(T)$.

5. CONCLUSIONS

Thus, the colossal magnetodielectric effect has been observed in $\text{SmFe}_3(\text{BO}_3)_4$; it is manifested in the (more than threefold) increase in the dielectric constant ε at $T < T_N$ and its suppression to the primary level of the paramagnetic state in the magnetic field of $\sim 5 \text{ kOe}$ applied in the basal crystal ab plane. It has been established that the observed behavior of ε closely correlates with the spontaneous and field-induced electric polarizations. The theoretical explanation of the observed phenomena has been proposed. It has been shown that the observed magnetodielectric effect is due to the contribution to the dielectric constant ε from the electric susceptibility related to the rotation of spins in the ab plane upon the antiferromagnetic ordering of the Fe^{3+} ions, which is suppressed by the magnetic field. Its high value in samarium ferroborate $\Delta\varepsilon \sim (P_{\perp}^0)^2/K$ is explained by the relatively high electric polarization P_{\perp}^0 in the basal plane. In the easy-plane state, this polarization easily rotates in the electric field due to the low magnetic-anisotropy energy K in the basal plane. A theoretical model is elaborated, which consistently describes the main features of the behavior of the dielectric constant and electric polarization in the magnetic field taking into account the induced magnetoelastic anisotropy in the basal plane. The analysis of the temperature dependences of the observed phenomena allowed the establishment of the prevailing contribution of the rare-earth (Sm) subsystem to the considered effects.

A strong magnetodielectric effect was recently observed in $\text{HoFe}_3(\text{BO}_3)_4$ ferroborate [11]. We suppose that the mechanism of its origin is similar to that proposed above; i.e., it is due to the rotation electric susceptibility in the ab plane. The relatively low value of the magnetodielectric effect in other ferroborates (see, e.g., [12]) is apparently related to the low polarization value, taking into account that $\varepsilon \sim (P_{\perp}^0)^2$.

The mechanism of the appearance of the “rotational” dielectric contribution considered in this work

may generally exist in a wide class of multiferroics having spontaneous polarization of the improper origin related to their magnetic structure.

We are grateful to A.K. Zvezdin and A.P. Pyatakov for the discussion of this work and valuable comments. This work was supported by the Russian Foundation for Basic Research, project nos. 10-02-00846 and 09-02-01355.

REFERENCES

1. M. Fiebig, *J. Phys. Appl. Phys.* **38**, R123 (2005).
2. Y. Tokura, *Science* **312**, 1481 (2006).
3. S.-W. Cheong and M. Mostovoy, *Nature Mater.* **6**, 13 (2007).
4. D. Khomskii, *J. Magn. Magn. Mater.* **306**, 1 (2006).
5. R. Ramesh and N. A. Spaldin, *Nature Mater.* **6**, 21 (2007).
6. T. Kimura, T. Goto, H. Shintani, et al., *Nature* **426**, 55 (2003).
7. T. Goto, T. Kimura, G. Lawes, et al., *Phys. Rev. Lett.* **92**, 257201 (2004); T. Kimura, J. C. Lashley, and A. P. Ramirez, *Phys. Rev.* **73**, 220401 (2006).
8. A. K. Zvezdin, S. S. Krotov, A. M. Kadomtseva, et al., *Pis'ma Zh. Eksp. Teor. Fiz.* **81**, 335 (2005) [JETP Lett. **81**, 272 (2005)].
9. A. K. Zvezdin, G. P. Vorob'ev, A. M. Kadomtseva, et al., *Pis'ma Zh. Eksp. Teor. Fiz.* **83**, 600 (2006) [JETP Lett. **83**, 509 (2006)].
10. A. N. Vasil'ev and E. A. Popova, *Fiz. Nizk. Temp.* **32**, 968 (2006) [*J. Low Temp. Phys.* **32**, 735 (2006)].
11. R. P. Chaudhury, F. Yen, B. Lorenz, et al., *Phys. Rev. B* **80**, 104424 (2009).
12. A. M. Kadomtseva, Yu. F. Popov, G. P. Vorob'ev, et al., *Fiz. Nizk. Temp.* **36**, 640 (2010) [*J. Low Temp. Phys.* **36**, 532 (2010)].
13. Yu. F. Popov, A. P. Pyatakov, A. M. Kadomtseva, et al., *Zh. Eksp. Teor. Fiz.* **138**, 226 (2010) [*J. Exp. Theor. Phys.* **111**, 199 (2010)].
14. A. K. Zvezdin, R. Z. Levitin, A. I. Popov, et al., *Zh. Eksp. Teor. Fiz.* **80**, 1504 (1981) [*Sov. Phys. JETP* **53**, 771 (1981)].
15. G. A. Babushkin, A. K. Zvezdin, R. Z. Levitin, et al., *Zh. Eksp. Teor. Fiz.* **85**, 1366 (1983) [*Sov. Phys. JETP* **58**, 792 (1983)].
16. A. K. Zvezdin, V. M. Matveev, A. A. Mukhin, and A. I. Popov, *Rare-Earth Ions in Magnetically Ordered Crystals* (Nauka, Moscow, 1985) [in Russian].
17. E. P. Chukalina, M. N. Popova, L. N. Bezmaternykh, and I. A. Gudim, *Phys. Lett. A* **374**, 1790 (2010).

Translated by L. Mosina